Chinese Chemical Letters 34 (2023) 107466

Contents lists available at ScienceDirect

Chinese Chemical Letters

journal homepage: www.elsevier.com/locate/cclet

The role of externally-modulated electrostatic interactions in amplifying charge transport across lysine-doped peptide junctions

Xiaobing Li[a,1], Pierre-André Cazade[b,1], Pan Qi[a], Damien Thompson[b,*], Cunlan Guo[a,*]

[a] College of Chemistry and Molecular Sciences, Wuhan University, Wuhan 430072, China
[b] Department of Physics, Bernal Institute, University of Limerick, Limerick V94 T9PX, Ireland

ARTICLE INFO

Article history:
Received 18 January 2022
Revised 21 February 2022
Accepted 24 April 2022
Available online 28 April 2022

Keywords:
Bioelectronics and biosensors
Charge transport
Linear peptide
Protonation
Self-assembled monolayer

ABSTRACT

Many evolved biomolecular functions such as ion pumping or redox catalysis rely on controlled charge transport through the polypeptide matrix, which can be regulated by shifts in molecular protonation states and dependent supramolecular packing modes in response to environmental cues. However, the exact roles of such dynamic, non-covalent interactions in peptide charge transport have remained elusive. To tackle this challenge, here we report the modulation of charge transport in a series of lysine (Lys)-substituted hepta-glycine (Gly) peptide self-assembled monolayers (SAMs) on template-striped gold (Au^{TS}) bottom electrodes with eutectic gallium-indium (EGaIn) liquid metal top electrodes. We demonstrate systematic modulation of hydrogen bonding and more general electrostatic interactions by shifting the position of the charged Lys-residue and creating different protonation patterns by changing the environmental pH in the Au^{TS}/peptide//GaO_x/EGaIn junctions. The effective modulation is evidenced by current density–voltage (*J-V*) measurements combined with SAM characterization using ultraviolet photoelectron spectroscopy (UPS) and angle-resolved X-ray photoelectron spectroscopy (ARXPS), polarization modulation–infrared reflection-absorption spectroscopy (PM-IRRAS), and molecular dynamics (MD) simulations. Decreasing the hydrogen bonding inside the peptide SAMs and increasing the electrostatic interactions by environmental counterions amplifies the charge transport differently with Lys-position, which means that the sensitive electrical response of peptide SAMs can be tuned by the peptide sequence. Our results provide insights into the relationship between molecular design and *in situ* modulation of charge transport properties for the development of bionanoelectronics.

Non-covalent interactions direct the self-assembly of biomolecules into complex functional architectures, which are essential to maintain the delicate structures and diverse functions of proteins inside cells. Moreover, non-covalent interactions are known to regulate charge transfer involved in biologically important processes such as enzymatic catalysis and signal transduction [1–5], and are the key to rational design of molecular devices and sensors. Proteins self-assemble and pack together using hydrogen bonds and more general electrostatic interactions, van der Waals (vdW) contacts, and hydrophobic interactions, which are created by the charged, polar, and hydrophobic amino acid residues [6–8]. These dynamic binding interactions can be switched on and off by environmental triggers to realize protein function [8–10]. Charge transfer through the peptide matrix will be sensitive to the presence and position of charged or polar groups but it is difficult to predict *a priori* the exact effect of a given change in molecular structure or environment on charge transport, which is critical for the rational design and performance optimization of peptide/protein based biosensors [11–13]. Deeper insight into structure-function relations in peptide junctions would aid efforts to design bioelectronics in different environments from vacuum to water to complex bio-fluids.

To distinguish the roles of the various competing non-covalent interactions in the regulation of charge transport in peptides, we synthesized a series of lysine (Lys)-doped linear oligo-peptides as a model system. The Lys side chain ε-ammonium group is positively charged at neutral pH and is a key building block [14–16] as a hydrogen bond donor [17,18] and a creator of salt bridges with negatively charged residues [19] and cation-π interactions with aromatic phenylalanine, tryptophan, and tyrosine residues [20]. The Lys residue shifts between protonated ammonium ($R\text{-}NH_3^+$) and neutral amine ($R\text{-}NH_2$) for different protein behaviors [21,22]. The dynamic pK_a-based switching provides a means of altering the

* Corresponding authors.
E-mail addresses: damien.thompson@ul.ie (D. Thompson), cunlanguo@whu.edu.cn (C. Guo).
[1] These authors contributed equally to this work.

https://doi.org/10.1016/j.cclet.2022.04.064
1001-8417/

protein function by rerouting charge transport [23–25] simply by changing the acidity of the environment.

In this work, we designed a series of hetero-hepta-glycine (Gly, G) self-assembled monolayers (SAMs) doped with a single Lys at the bottom, middle, or top of the SAM. By switching the environment among alkaline, neutral, and acidic conditions, the properties of the peptide SAMs on template-stripped gold (Au^{TS}) can be controlled by modulating the net charge on Lys and the C-terminus. The corresponding charge transport through the peptide SAMs was characterized by constructing the Au^{TS}/peptide//GaO_x/EGaIn junctions with eutectic indium-gallium liquid metal top-electrodes (EGaIn). We benchmarked molecular dynamics (MD) models using physicochemical characterization of the SAMs under different conditions by angle-resolved X-ray photoelectron spectroscopy (ARXPS) and polarization modulation–infrared reflection-absorption spectroscopy (PM-IRRAS). The non-covalent interactions inside the SAMs as well as between SAMs and environmental counterions, including hydrogen bonding networks, more general electrostatic interactions, and vdW interactions, were then mapped with the models. The data shows that the charge transport can be amplified by reducing hydrogen bonding and electrostatic interactions inside the SAMs (including intra- and inter-peptide contacts) and increasing the binding strengths between the SAM and the environmental counterions, which can be achieved by moving the Lys group from the bottom to the top of the SAM and changing the environment. The demonstrated control of the subtle balance between hydrogen bonding and more general electrostatics in the SAMs helps to explain the relationship between the peptide structure and charge transport. It also provides a path to tailoring peptide sequence to generate or detect sensitive electrical response, which provides new strategies for the development of cost-effective, sustainable, biocompatible peptide-based devices [26].

The freshly prepared Au^{TS} substrate was incubated in peptide solution overnight and then washed with H_2O, followed by nitrogen drying to construct peptide SAMs. The peptide SAMs were characterized by atomic force microscopy (AFM), ellipsometry, ARXPS, PM-IRRAS, and UPS to measure their morphology, thickness, coverage, chemical structure. MD simulations were performed to predict the packing modes of the peptides in the SAMs and quantify the non-covalent interactions. The peptide SAMs were contacted with cone-shaped GaO_x/EGaIn tips to form the Au^{TS}/peptide//GaO_x/EGaIn junctions for current-voltage measurements. The full details of the experimental and modeling methods are provided in Supporting information.

We designed three linear hepta-peptides comprised of six Gly and one Lys (Fig. 1A). Mercaptopropionic acid (MPA) was covalently conjugated at the N-terminus of each peptide to facilitate anchoring of the peptide SAMs on the gold bottom-electrodes *via* Au-S bonding. The carboxylate group (COO^-) of the C-terminus at the other end of the peptide and the amino group (NH_3^+) of the Lys side chain can exchange labile protons with environmental water under acidic and alkaline conditions. The Lys was located at the N-terminus (K-1) at the bottom of the SAM, in the middle of the SAM (K-4), or the C-terminus (K-7) at the top of the SAM, to place the carboxylate and amino groups in a series of far, medium, and close distances to evaluate the effect of Lys position on electrostatic interactions. The reference lysine-free hepta-7Gly (7G, Fig. S1 in Supporting information) SAM was used as a control.

All the peptide SAMs display uniform morphologies on the Au^{TS} surface as characterized by AFM (Fig. S2 in Supporting information). The thickness of peptide SAMs from ellipsometry is in the range of 20–30 Å (Table S1 in Supporting information), similar to reported thicknesses of hepta-peptides [27–29]. Among them, K-1, K-4 and 7G display slightly lower thickness than the theoretical length under fully extended conformation (30 Å), which

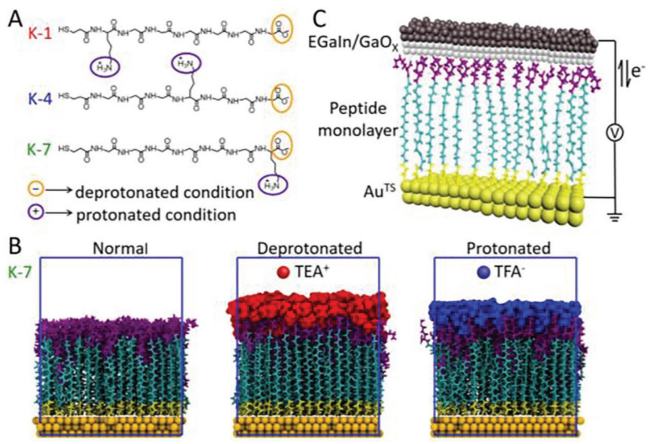

Fig. 1. Scheme of the experimental setup. (A) Structures of peptides studied. K-1: MPA-KGGGGGG; K-4: MPA-GGGKGGG; K-7: MPA-GGGGGGK (G = glycine, K = lysine). MPA is attached to the N-terminal of the peptide. The orange and blue circles label the titratable groups that switch between deprotonated and protonated conditions. (B) Computed molecular structures of the K-7 peptide SAMs in normal, deprotonated, and protonated states following 10 ns of free dynamics. Gold atoms are depicted as orange spheres, TEA^+ molecules as red spheres, and TFA^- molecules as blue spheres. The peptides are depicted with sticks. Lys residues are shown in purple, Gly residues in cyan, and MPA residues in yellow. (C) Schematic illustration of the Au^{TS}/peptide//GaO_x/EGaIn junction setup.

is due to the tilt or some back-bending of the residues in the SAMs [27]. The molecular coverage of peptide SAMs (Table S2 in Supporting information) from ARXPS (Fig. S3 in Supporting information) is in the range of 10^{-10} mol/cm^2 with an order of K-7 > K-4 > K-1, consistent with the measured heights. Moreover, the peptide coverage is on the same order of magnitude as unfunctionalized alkanethiol SAMs [30,31], and, *e.g.*, ferrocene- and viologen-functionalized alkanethiol SAMs [32–34], indicating that the peptide molecules assemble in densely-packed, upright SAMs. The PM-IRRAS spectra further confirmed the successful assembly of peptide molecules on the Au surface with the amide I and II modes in the range of ~1664 and 1562 cm^{-1} (Fig. S4 in Supporting information) [35,36].

The isoelectric points (pI) of the three hepta-peptides are ~8.5. Under normal conditions, the C-terminus and Lys-residue are in the forms of $-COO^-$ and $-NH_3^+$, respectively, creating a zwitterion. The C-terminus and Lys residue converted into deprotonated $-COO^-$ and $-NH_2$ under alkaline conditions and into protonated –COOH and $-NH_3^+$ in acidic conditions [37,38]. We treated the peptide SAMs with triethylamine (TEA) or trifluoroacetic acid (TFA). The TEA^+ or TFA^- counterions could adsorb on top of the peptide SAMs to balance the charges (Fig. 1B). The obtained peptide SAMs do not have obvious changes in the thickness measured by ellipsometry (Table S1), nor in the morphologies by AFM (Fig. S5 in Supporting information). As shown in PM-IRRAS (Fig. S6 and Table S3 in Supporting information), the protonation in acid produces a blue shift in the amide I peak for K-1 and K-7, but not K-4. After the deprotonation in alkaline conditions, the amide peak positions barely shift, but the amide I/II ratio values increase largely for K-1, less for K-4, and with no significant change for K-7. The above results indicate that the peptide structure changes in two different ways under acidic and alkaline conditions. The position of Lys in the peptide also influences the response of the peptide structure to different conditions. In this way, the delicate balance of SAM and SAM–environment non-covalent interactions can be modulated.

We constructed the Au^{TS}/peptide//GaO_x/EGaIn junctions by placing the EGaIn/GaO_x tip on top of the peptide SAMs following reported methods (Fig. 1C) [39]. A total of 600–1000 current density–voltage *J-V* curves were recorded by biasing

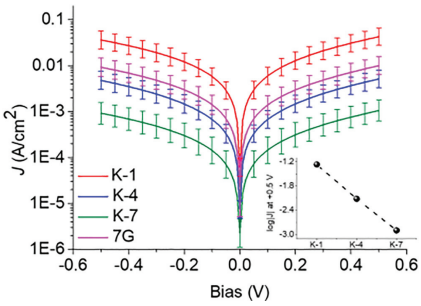

Fig. 2. Current density-voltage plots for peptide junctions of K-1, K-4, K-7, and 7G under normal condition. Inset: the trend of current density with Lys position at + 0.5 V for peptide SAM junctions.

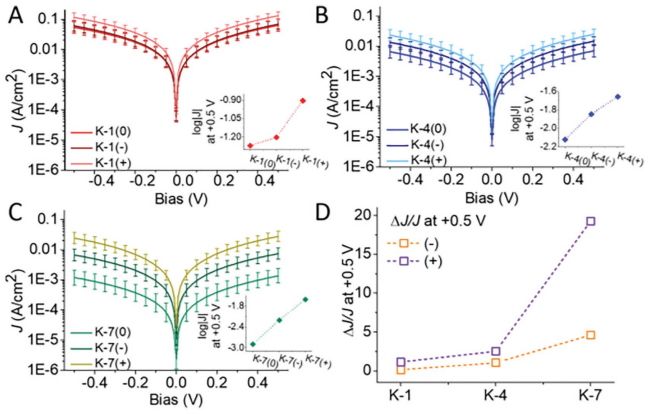

Fig. 3. Current density-voltage plots of peptide junctions under normal, deprotonated, and protonated conditions: (A) K-1, (B) K-4 and (C) K-7. Insets: Trends of current density with different conditions at + 0.5 V. (D) Plot of $\Delta J/J$ at + 0.5 V *vs.* the Lys position in peptide SAMs. ΔJ is the change in current density under deprotonated or protonated conditions compared with the normal condition where J is the current density under normal condition. (0): normal, (-): deprotonated, (+): protonated.

the peptide SAM junctions and the current density values at +0.5 V were collected to quantify the statistics of conductance among peptide SAMs (Fig. S7 in Supporting information). The normal peptide junctions show conductance of K-1 > K-4 > K-7 in a near-linear relationship (Fig. 2). Among them, the K-4 SAM shows a similar thickness to the reference Lys-free 7G SAM and a slightly lower conductance than 7G, indicating that the mere presence of Lys does not dramatically change the charge transport of poly-Gly. The conductance differences among these K-peptides reflect the change in SAM electronic and physical structure with the Lys-position, and the conductance differences could come from the combination of SAM thickness (barrier height for tunneling) and peptide disorder (path lengths for incoherent tunneling or efficiency of inter-peptide charge transfer).

The peptide SAMs were then treated with acid or alkali to assess the tunability of peptide interactions for environmental control of charge transport through the junction (Fig. 3). Both the protonation and deprotonation increase the peptide charge transport in the trend of J (protonated) > J(deprotonated) > J(normal). Meanwhile, the changes of current density (shown as $\Delta J/J$) gradually increase (Fig. 3D) as Lys-moves from position 1 to 7 (*i.e.*, as Lys is shifted from the bottom to the top of the SAM, Fig. 1A). Hence, the current amplification in the peptide SAM junction can be obtained by both the protonation/deprotonation and the peptide sequence. Interestingly, the $\Delta J/J$ values of K-7, *i.e.*, with Lys at the top of the SAM, have the largest change under deprotonated and protonated conditions compared with K-1 and K-4.

To understand the current density increases of protonated and deprotonated hepta-peptide junctions compared to the normal

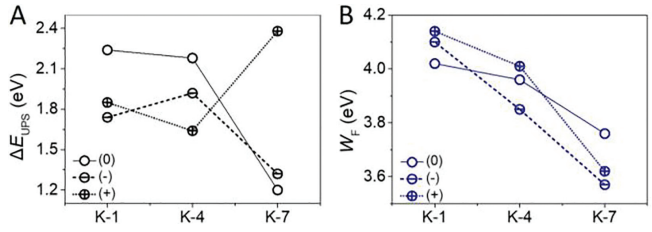

Fig. 4. Comparison of peptide–electrode energy offset (ΔE_{UPS}) (A) and work function (W_F) (B) of peptide SAMs on Au^{TS} from UPS measurements. The trend of ΔE_{UPS} (A) and W_F (B) are for peptide SAMs with the Lys position shifting from 1 to 7.

one, we first characterized the energy landscape of the peptide SAMs under these three conditions using UV photoelectron spectroscopy (UPS) (Figs. 4 and S8 in Supporting information) [40]. The peptide–electrode energy offsets ΔE_{UPS} range from 1.20 eV to 2.38 eV for the three Lys-substituted peptide SAMs under the different conditions, but do not have clear trends with either the protonation state or Lys position, or with the charge transport properties of the peptide SAMs (Fig. 4A). The work function (W_F) varies with the Lys-position and is higher after protonation than after deprotonation (Fig. 4B). Generally, the W_F values are sensitive to the peptide–electrode interaction, surface polarization, and dipole interactions of peptides, which are related to peptide structure [41–43]. Here, different W_F shifts indicate various effects of the peptide on the electrode during the (de)protonation process, which also mean corresponding energy and structure changes among peptides in this process. Notably, these overall W_F shifts are also not consistent with the changes of peptide charge transport. Therefore, we reason that factors other than the overall ΔE_{UPS} or W_F shift, such as packing interactions in the SAM, contribute to the measured changes in charge transport.

To understand the possible factors related to the changes of charge transport, we modeled the structure of peptide SAMs under normal, deprotonated, and protonated conditions using room temperature MD simulations (Fig. 1B and Fig. S9 in Supporting information). The modeled peptide SAMs displayed a thickness trend of K-1 < K-4 < K-7, consistent with the ellipsometry results (Fig. S10 in Supporting information). The thickness from MD simulation does not show a unified trend due to the specificity of K-7 for which Lys is the terminal group. $-COO^-$ and $-NH_3^+$ groups are both close to the top of the SAM and will be the defining factor of the SAM height depending on the protonation state. For the normal and deprotonated SAMs, $-COO^-$ drives the height. As the peptide is already stretched to its full extent due to molecular packing, adding positive counterions can hardly force the $-COO^-$ group to stretch further up. However, for the protonated SAM, the long Lys side chain which carries the $-NH_3^+$ is free to extend further up to form complex with the negative counterions on top of the SAM. The increase trend of current cannot be solely explained by the variation in the SAM height. Hence the structural and energetic analyses are discussed below in detail. In particular, as molecular self-assembly is directed by the formation of hydrogen bonds, electrostatic interactions, and vdW interactions [44–46], we evaluated the incidence, dynamics, and energetics of these interactions that are related to the peptide conformation and further the charge transport of peptide SAMs [32,34,47,48].

The N–O separation was mapped between the nitrogen atom of the Lys side chain and the oxygen atom at the C-terminus within each peptide (intra-molecular) and between different peptide molecules (inter-molecular) (Fig. S11 in Supporting information). For all the three peptides in normal condition, a sharp first peak at ~3 Å was observed for intra-molecular N–O distances, but a much broader, disordered distribution was computed for the inter-molecular N–O distances. Due to the flexibility of

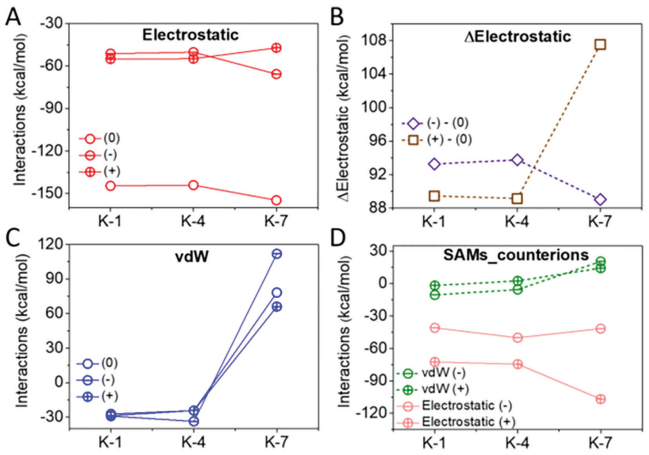

Fig. 5. Calculated supramolecular packing energies as a function of the Lys position in the SAM as determined from molecular dynamics simulations. (A) The electrostatic interactions in peptide SAMs under different conditions. (B) The differences of the electrostatic interactions between (de)protonated and normal conditions where (de)protonated – normal = Δelectrostatic. (C) The vdW interactions in peptide SAMs under different conditions. (D) The electrostatic interactions between the peptide SAMs and environmental counterions under deprotonated and protonated conditions.

the peptides, the Lys side chain can directly interact with the C-terminus in peptide molecule, regardless of Lys-position shifts (Fig. S12 in Supporting information). The contact distance is in good agreement with known hydrogen bond lengths for amino–carboxylate interactions (2.8–3.0 Å) [49–52]. These well-defined hydrogen bonds only exist within each peptide molecule (Fig. S11, gray histograms), but not between peptide molecules (Fig. S11, red distribution). Furthermore, the population of N—O separations around 3 Å markedly decreases after (de)protonation treatments for all three peptide SAMs. This suggests a decrease in the interaction between Lys side chain and the C-terminus and/or a steric hindrance establishes this specific hydrogen bond after (de)protonation. The *J-V* response of the peptide junctions is enhanced after (de)protonation, which suggests that freeing the C-terminus and Lys side chain from intramolecular hydrogen bonds increases charge transport.

We further characterized the packing energies of the SAMs as the combination of peptide-peptide and peptide-counterion electrostatic and vdW interactions (Figs. S13 and S14 in Supporting information). Note the MD structures show that TEA^+ cannot penetrate the SAMs, while TFA^- penetrates the K-1 and K-4 but not the ordered, fully-upright K-7 SAM (Fig. S9). The total packing energies are comparable for protonated and neutral SAMs, while the deprotonated SAMs pack more loosely (Fig. S15 in Supporting information). The peptide–peptide electrostatic interaction shows trends similar to that of the measured energy offsets ΔE_{UPS} (Figs. 4A and 5A). The variation of electrostatic interaction (Fig. 5B) tracks the measured current density (Fig. 3D), in particular for the protonated K-7 system with a sharp decrease of the peptide-peptide electrostatic interaction coinciding with the increase of current density. The reduced interaction inside the SAM is due to the competing attraction of the protonated K-7 for the counterions above the SAM, which reduces the Lys interaction with the C-terminus. Given that hydrogen bonds are generally the prime contributors to electrostatic interactions inside peptide SAMs, the weakened electrostatic interaction inside the SAM reflects the loss of hydrogen bonding. As the MD structures show that the side chain of Lys binds to counterions on the surface of the SAMs (Fig. S9), the internal Lys–C-terminus hydrogen bonds are removed to accelerate charge transport. Furthermore, decomposing the electrostatic interaction shows different proportions of peptide-peptide and peptide-counterion interactions among SAMs in alkaline, neutral and acidic environments (Figs. S13 and S14). For the neutral system, the C-terminus and Lys side chain in the forms of $–COO^-$ and $–NH_3^+$ make stronger peptide-peptide electrostatic interactions, while the protonation and deprotonation both weaken these interactions (Figs. 5A and B), matching with the loss of hydrogen bonds reported earlier. This is again consistent with the increasing current density for peptide junctions after (de)protonation treatment (Fig. 3D), showing that decreasing of peptide-peptide electrostatic interactions between key functional groups can promote charge transport across the peptide junctions. However, the changes of electrostatic interaction for K-1 and K-4 under different protonation conditions do not conform systematically with the changes of charge transport. This confirms the non-negligible role of secondary effects such as vdW interactions. Additionally, peptide–peptide vdW interactions were computed (Fig. 5C). K-1 and K-4 have minor vdW attractions in peptide SAMs, while K-7 shows net repulsion for all the normal, protonated, and deprotonated conditions. As expected for these polar SAMs, the changes of vdW interaction by (de)protonation are smaller than the electrostatic interactions for all the three peptide SAMs, reflecting the secondary influence of peptide–peptide vdW interaction.

We further detail the peptide–counterion interactions to capture the remaining electrostatic interactions in the junction (Fig. 5D and Fig. S14 in Supporting information). After the alkaline or acidic treatments, the counterions (TEA^+ or TFA^-) coordinate the top of the SAM with the degree of penetration depending on the location of the complementary charged sites in the SAM molecules, the order of the SAM packing, and the size of the counterion. The peptide–counterion vdW interactions are almost the same between protonated and deprotonated conditions. The electrostatic peptide(+)-TFA^- interactions are stronger than peptide(−)-TEA^+, reflecting the stronger burrowing of the smaller TFA^- molecule into the SAMs. These electrostatic peptide(+)-TFA^-interactions also increase in a trend of K-7 > K-4 > K-1, which is similar to that of the charge transport. It indicates that promoting peptide–counterion interaction in order to reduce the competing peptide–peptide interaction could efficiently facilitate the charge transport of the peptide junctions, which is also one of the reasons for the difference of $\Delta J/J$ between protonated and deprotonated peptide junctions. The current densities of K-1 and K-4 molecular junctions change little when the external environment changes. Our data indicates that this is because the Lys side chain is buried and so, unlike K-7, the peptide-counterions interactions that boost current density are hindered in the (de)protonated within the K-1 and K-4 peptide SAMs. The counterions may help order the SAM molecules in more upright orientations [34,53], as shown for example here for protonated K-7, and may create tighter seals between the SAM and the Ga_2O_3 top-electrode surface [54]. The comparisons between the models and electrical measurements indicate that the balance between internal and external SAM interactions is the main driving force behind the response of the junctions to protonation state, providing a means of optimizing the charge transport across peptide junctions by changing the charge state of molecules (here, explored by the changing Lys position and the type of counterion) and consequent SAM packing mode.

The charge transport of various molecular SAMs composed of a broad range of chemical moieties including aliphatic hydrocarbon and aromatic linkers with functional groups (usually but not always the terminal group) of organometallics and charged/redox units have been compared in EGaIn//SAM-metal junctions, which indicated that the charge transport is dominated by the SAMs, not the SAM-EGaIn coupling [55–57]. Some electrostatic EGaIn//SAM effects have been observed [47,58], including for SAMs with buried redox units [33], but appear to be non-specific, field-based coupling. Here, our measured charge transport variations of peptide

junctions can be related to peptide-counterions electrostatic interactions, suggesting that the coupling between peptides and EGaIn is relatively weak. In earlier studies of Au-peptide-Au junctions, the coupling between peptides and Au could be critical for the charge transport, which depends on the peptide composition [27].

From the above discussions, hydrogen bonds and, more generally, electrostatic interactions are the primary means of regulating the charge transport through peptide SAM junctions. Weakening hydrogen bonding inside the SAMs can improve the charge transport, and this is further promoted by interactions with counterions that mostly sit on top of the SAM. It was recently reported that peptide hydrogen bonds can accelerate the charge transport through oligo-peptide conjugates in an organic solution [59] and amyloid crystals in a dry condition [60]. Here our work demonstrates that external electrostatic attractions between peptides and environmental ions can provide compensating, pH-controllable interactions that also modulate peptide charge transport. Reconciling the measured charge transport with the molecular models indicates that the Lys position is a key factor of the electrical properties, engaging in hydrogen bonding inside the SAM and electrostatic interactions with the counterions.

In this work, we focus on the sensitive response of peptide charge transport to protonation in solid-state junctions, which is finely controlled by the composition and structure of peptide SAMs. The simple presence of Lys in the peptide sequence does not dramatically improve the charge transport in net neutral oligopeptide SAM junctions but can controllably amplify the charge transport by reacting to surrounding conditions which in turn depends on its position in the SAM. Non-covalent interactions have a large influence on the charge transport response, especially hydrogen bonding inside the SAM and electrostatic interactions between the SAM and environmental counterions. These interactions can be finely tuned by the position of Lys, the protonation state, and the type of counterions, showing controllable response beyond just the simple design of hydrogen bonding networks alone [59,60]. Our results show that peptide junctions with polar or charged groups at the top of the SAMs can modulate charge transport according to the environmental dynamics. It would be interesting to test in future work if the observed current regulation holds for different peptide lengths and backbone sequences, including also further exploration of the (de)protonation response of labile groups for environment-based modulation of charge transport in peptide junctions. Our work suggests an avenue toward the rational design of hetero-peptide SAMs with orthogonally controllable electronic properties for responsive devices.

Declaration of competing interest

The authors declare that they have no known competing financial interests or personal relationships that could have appeared to influence the work reported in this paper.

Acknowledgments

This work was supported by the National Natural Science Foundation of China (Nos. 21974102 and 21705019) and the National Key R & D Program of China (No. 2018YFA0703700). D.T. acknowledges support from Science Foundation Ireland (SFI, No. 12/RC/2275_P2) and supercomputing resources at the SFI/Higher Education Authority Irish Center for High-End Computing (ICHEC).

Supplementary materials

Supplementary material associated with this article can be found, in the online version, at doi:10.1016/j.cclet.2022.04.064.

References

[1] H.B. Gray, J.R. Winkler, Q. Rev. Biophys. 36 (2003) 341–372.
[2] D.N. Beratan, C.R. Liu, A. Migliore, et al., Acc. Chem. Res. 48 (2015) 474–481.
[3] V.L. Davidson, Acc. Chem. Res. 41 (2008) 730–738.
[4] J. Qin, A.M. Gronenborn, FEBS J. 281 (2014) 1948–1949.
[5] R.N. Perham, Annu. Rev. Biochem. 69 (2000) 961–1004.
[6] A.H. Mao, S.L. Crick, A. Vitalis, et al., Proc. Natl. Acad. Sci. U. S. A. 107 (2010) 8183–8188.
[7] M. Bhattacharyya, S. Ghosh, S. Vishveshwara, Curr. Protein Pept. Sci. 17 (2016) 4–25.
[8] B. Yu, C.C. Pletka, J. Iwahara, Proc. Natl. Acad. Sci. U. S. A. 118 (2021) e2015879118.
[9] B.S. Ibrahim, V. Pattabhi, Biochem. Biophys. Res. Commun. 325 (2004) 1082–1089.
[10] H.X. Zhou, X. Pang, Chem. Rev. 118 (2018) 1691–1741.
[11] B. Viguier, K. Zor, E. Kasotakis, et al., ACS Appl. Mater. Interfaces 3 (2011) 1594–1600.
[12] N. Liu, N. Hui, J.J. Davis, et al., ACS Sens. 3 (2018) 1210–1216.
[13] E. Palecek, J. Tkac, M. Bartosik, et al., Chem. Rev. 115 (2015) 2045–2108.
[14] D. Datta, A. Bhinge, V. Chandran, Cytotechnology 36 (2001) 3–32.
[15] G.P. Maier, M.V. Rapp, J.H. Waite, et al., Science 349 (2015) 628–632.
[16] C. Azevedo, A. Saiardi, Adv. Biol. Regul. 60 (2016) 144–150.
[17] G.H. Li, L. Feng, P.N. Zhao, et al., J. Colloid Interface Sci. 431 (2014) 233–240.
[18] M. Suzuki, H. Saito, K. Hanabusa, Langmuir 25 (2009) 8579–8585.
[19] J.P. Gallivan, D.A. Dougherty, J. Am. Chem. Soc. 122 (2000) 870–874.
[20] J.P. Gallivan, D.A. Dougherty, Proc. Natl. Acad. Sci. U. S. A. 96 (1999) 9459–9464.
[21] D.G. Isom, C.A. Castaneda, B.R. Cannon, et al., Proc. Natl. Acad. Sci. U. S. A. 108 (2011) 5260–5265.
[22] M.J. Matos, B.L. Oliveira, N. Martinez-Saez, et al., J. Am. Chem. Soc. 140 (2018) 4004–4017.
[23] K. Kapoor, D.J. Cashman, L. Nientimp, et al., J. Phys. Chem. B 122 (2018) 1026–1036.
[24] N. Fischer, M. Hippler, P. Setif, et al., EMBO J. 17 (1998) 849–858.
[25] A.A. Yunus, C.D. Lima, Nat. Struct. Mol. Biol. 13 (2006) 491–499.
[26] K. Tao, P. Makam, R. Aizen, et al., Science 358 (2017) eaam9756.
[27] C.L. Guo, X. Yu, S. Refaely-Abramson, et al., Proc. Natl. Acad. Sci. U. S. A. 113 (2016) 10785–10790.
[28] L. Sepunaru, S. Refaely-Abramson, R. Lovrincic, et al., J. Am. Chem. Soc. 137 (2015) 9617–9626.
[29] B.L. Li, X. Ji, L.X. Tian, et al., Chin. Chem. Lett. 32 (2021) 3782–3786.
[30] M.M. Walczak, D.D. Popenoe, R.S. Deinhammer, et al., Langmuir 7 (1991) 2687–2693.
[31] D.E. Weisshaar, M.M. Walczak, M.D. Porter, Langmuir 9 (1993) 323–329.
[32] Y.M. Han, C. Nickle, Z.Y. Zhang, et al., Nat. Mater. 19 (2020) 843–848.
[33] Y. Li, N. Nerngchamnong, L. Cao, et al., Nat. Commun. 6 (2015) 6324.
[34] N. Nerngchamnong, Y. Li, D.C. Qi, et al., Nat. Nanotechnol. 8 (2013) 113–118.
[35] M. Baghbanzadeh, C.M. Bowers, D. Rappoport, et al., Angew. Chem. Int. Ed. 54 (2015) 14743–14747.
[36] C.L. Guo, J.X. Yu, J.R. Horsley, et al., J. Phys. Chem. B 123 (2019) 10951–10958.
[37] N. Kitadai, T. Yokoyama, S. Nakashima, J. Colloid Interface Sci. 329 (2009) 31–37.
[38] V. Humblot, C. Methivier, C.M. Pradier, Langmuir 22 (2006) 3089–3096.
[39] R.C. Chiechi, E.A. Weiss, M.D. Dickey, et al., Angew. Chem. Int. Ed. 47 (2008) 142–144.
[40] Y. Li, R. Breuer, J. Li, et al., Nano Lett. 15 (2015) 5506–5512.
[41] K. Michaeli, N. Kantor-Uriel, R. Naaman, et al., Chem. Soc. Rev. 45 (2016) 6478–6487.
[42] X.Y. Deng, R.M. Nie, A.Y. Li, et al., Adv. Mater. Interfaces 1 (2014) 1400215.
[43] C. Shlizerman, A. Atanassov, I. Berkovich, et al., J. Am. Chem. Soc. 132 (2010) 5070–5076.
[44] A. Tkatchenko, M. Scheffler, Phys. Rev. Lett. 102 (2009) 073005.
[45] S. Casalini, C.A. Bortolotti, F. Leonardi, et al., Chem. Soc. Rev. 46 (2017) 40–71.
[46] S. Zhang, Nat. Biotechnol. 21 (2003) 1171–1178.
[47] X.P. Chen, M. Roemer, Y. Li, et al., Nat. Nanotechnol. 12 (2017) 797–803.
[48] L. Belding, S.E. Root, Y. Li, et al., J. Am. Chem. Soc. 143 (2021) 3481–3493.
[49] S.Q. Ma, X.Q. Liu, Y.H. Jiang, et al., Sci. China Chem. 57 (2013) 379–388.
[50] S.Y. Sheu, D.Y. Yang, H.L. Selzle, Proc. Natl. Acad. Sci. U. S. A. 100 (2003) 12683–12687.
[51] C.C. Stephanie, van der Lubbe, F. Zaccaria, et al., J. Am. Chem. Soc. 141 (2019) 4878–4885.
[52] S.C.C. van der Lubbe, C. Fonseca Guerra, Chem. Asian J. 14 (2019) 2760–2769.
[53] S. Ye, Y. Sato, K. Uosaki, Langmuir 13 (1997) 3157–3161.
[54] D. Thompson, C.A. Nijhuis, Acc. Chem. Res. 49 (2016) 2061–2069.
[55] W.F. Reus, M.M. Thuo, N.D. Shapiro, et al., ACS Nano 6 (2012) 4806–4822.
[56] L. Cademartiri, M.M. Thuo, C.A. Nijhuis, et al., J. Phys. Chem. C 116 (2012) 10848–10860.
[57] K.S. Wimbush, R.M. Fratila, D. Wang, et al., Nanoscale 6 (2014) 11246–11258.
[58] M. Carlotti, A. Kovalchuk, T. Wachter, et al., Nat. Commun. 7 (2016) 13904.
[59] R. Orlowski, J.A. Clark, J.B. Derr, et al., Proc. Natl. Acad. Sci. U. S. A. 118 (2021) e2026462118.
[60] C. Shipps, H.R. Kelly, P.J. Dahl, et al., Proc. Natl. Acad. Sci. U. S. A. 118 (2021) e2014139118.